

## VERIFICATIONS OF SCALING RELATIONS USEFUL FOR THE INTRINSIC ALIGNMENT SELF-CALIBRATION

XIAN-GUANG MENG<sup>1,2</sup>, YU YU<sup>3,4,\*</sup>, PENGJIE ZHANG<sup>3,4,5,6</sup>, YIPENG JING<sup>3,4,5,6</sup>

*Draft version April 4, 2022*

### ABSTRACT

The galaxy intrinsic alignment (IA) is a major challenge of weak lensing cosmology. To alleviate this problem, Zhang (2010, MNRAS, 406, L95) proposed a self-calibration method, independent of IA modeling. This proposal relies on several scaling relations between two-point clustering of IA and matter/galaxy fields, which were previously only tested with analytical IA models. In this paper, these relations are tested comprehensively with an  $N$ -body simulation of  $3072^3$  simulation particles and boxsize  $600h^{-1}$  Mpc. They are verified at the accuracy level of  $\mathcal{O}(1)\%$  over angular scales and source redshifts of interest. We further confirm that these scaling relations are generic, insensitive to halo mass, weighting in defining halo ellipticities, photo- $z$  error, and misalignment between galaxy ellipticities and halo ellipticities. We also present and verify three new scaling relations on the B-mode IA. These results consolidate and complete the theory side of the proposed self-calibration technique.

*Subject headings:* gravitational lensing: weak large-scale structure of universe methods: numerical

### 1. INTRODUCTION

The intrinsic alignment (IA) of galaxies, in particular, the spatially correlated component of galaxy shapes, is a major challenge of weak lensing cosmology (see Troxel & Ishak 2015 for a recent review). Depending on galaxy types, it may significantly contaminate cosmic shear measurement in several ways. For weak lensing two-point correlation or its corresponding power spectrum, IA directly induces the so-called II term, arising from the IA auto correlation. Furthermore, IA can be spatially correlated with the ambient density field and therefore spatially correlated with gravitational lensing. This induces the so-called GI term (Hirata & Seljak 2004). These contaminations have been predicted in various simulations (e.g. Croft & Metzler 2000; Heavens et al. 2000; Jing 2002; Heymans et al. 2006; Joachimi et al. 2013; Hilbert et al. 2017; Xia et al. 2017; Wei et al. 2018) and analytical modeling (e.g. Catelan et al. 2001; Crittenden et al. 2001; Lee & Pen 2001; Hirata & Seljak 2004; Bridle & King 2007; Hui & Zhang 2008; Schneider & Bridle 2010; Blazek et al. 2011, 2015, 2017; Joachimi et al. 2011; Tugendhat & Schäfer 2018). Furthermore, they have been detected in observations (Brown et al. 2002; Hirata et al. 2004; Mandelbaum et al. 2006; Hirata et al. 2007; Okumura & Jing 2009; Okumura et al. 2009; Joachimi et al. 2011; Mandelbaum et al. 2011; Singh et al. 2015; Singh

& Mandelbaum 2016; van Uitert & Joachimi 2017).

Therefore, a major task in weak lensing cosmology is to remove/alleviate IA. There have been various proposals. From the data side, the II term can be eliminated by removing close galaxy pairs with the aid of photo- $z$  information, or disregarding auto correlation within the same photo- $z$  bin (King & Schneider 2002, 2003; Heymans & Heavens 2003; Takada & White 2004; King 2005). However, this results in significant loss of information. Furthermore, it does not eliminate the GI term. From the IA theory side, one may adopt specific models of IA, and fit IA model parameters simultaneously with cosmological parameters. This approach has been applied in CFHTLenS, KiDS, and DES (e.g. Kirk et al. 2010; Heymans et al. 2013; Abbott et al. 2016; Hildebrandt et al. 2017; Joudaki et al. 2017; Troxel et al. 2017). The main problem is the induced dependence on IA modeling. The nulling technique avoids such model dependence, by introducing a redshift-dependent weighting scheme to suppress the IA contribution (Joachimi & Schneider 2008, 2009). However, by design, the same weighting results in significant loss of weak lensing information, in particular, its redshift dependence.

Zhang (2010a,b) proposed two self-calibration techniques of both the GI and II contamination. The key in these self-calibration techniques is the discovered scaling relations independent of IA modeling. These scaling relations connect statistics of IA spatial clustering with that of the galaxy number density field and the matter density field (gravitational lensing). Combining all observables (galaxy shapes and galaxy number density) available in the same weak lensing survey, these scaling relations allow for unique determination of GI, II, and the lensing power spectrum. These self-calibration techniques have been extended to three-point statistics (Troxel & Ishak 2012a,b,c, 2015). Recently Yao et al. (2017) showed that the self-calibration technique can indeed render the otherwise significant IA contamination insignificant, without sacrificing the lensing signal and cosmological information.

<sup>1</sup> Key Laboratory for Research in Galaxies and Cosmology, Shanghai Astronomical Observatory, Chinese Academy of Sciences, 80 Nandan Road, Shanghai, 200030, Peoples Republic of China

<sup>2</sup> University of Chinese Academy of Sciences, 19A Yuquan Road Beijing, China, 100049, Peoples Republic of China

<sup>3</sup> Department of Astronomy, School of Physics and Astronomy, Shanghai Jiao Tong University, Shanghai, 200240, Peoples Republic of China

<sup>4</sup> Shanghai Key Laboratory for Particle Physics and Cosmology, Peoples Republic of China

<sup>5</sup> IFSA Collaborative Innovation Center, Shanghai Jiao Tong University, Shanghai 200240, Peoples Republic of China

<sup>6</sup> Tsung-Dao Lee Institute, Shanghai 200240, Peoples Republic of China

\* yuyu22@sjtu.edu.cn

The scaling relations (Zhang 2010a,b; Troxel & Ishak 2012a,b,c, 2015) have only been verified with several analytical IA models. The next step is to verify them in more realistic situations. It is therefore the main goal of the current paper, to test the three scaling relations proposed in Zhang (2010b, hereafter Z10) with a high resolution  $N$ -body simulation of  $3072^3$  simulation particles. Observationally, the IA contamination may only be non-negligible for early-type galaxies. The observed GI and II can both be well explained by the spatially correlated halo ellipticities in  $N$ -body simulations, together with misalignment between ellipticities of galaxies and halos (Okumura & Jing 2009; Okumura et al. 2009). One can prove that the existence of galaxy misalignment does not affect the above scaling relations. We have randomly rotated halos to present the misalignment of galaxies, and it only suppresses the IA amplitude, which agrees with previous works (e.g. Joachimi et al. 2013). Therefore, we carry out direct tests of scaling relations for halo ellipticities and their validity automatically applies to realistic early-type galaxies. With the verification of these scaling relations, the self-calibration technique in Z10 is now complete from the theory side.

This paper is organized as follows. §2 describes the self-calibration technique. §3 describes the simulation and data analysis. §4 verifies the scaling relations proposed in Z10. Three new scaling relations are proposed and verified too. §5 discusses and summarizes.

## 2. THE SELF-CALIBRATION TECHNIQUE

Here we briefly summarize the self-calibration technique proposed in Z10. Conventional lensing tomography usually adopts coarse redshift bins of width  $\sim 0.2$ , comparable to photo- $z$  error of individual galaxies. Such a coarse bin size is sufficient for extracting the cosmological information in weak lensing, since the lensing kernel only varies slowly with redshift. However, it disregards information valuable for calibrating IA. Due to the large number of source galaxies, even much finer photo- $z$  bins (e.g. of width  $\sim 0.01$ ) may have millions of galaxies, and therefore can have sufficient S/N of diagnosing IA. The IA self-calibration utilizes such information. First, we split galaxies into redshift bins of narrow width  $\mathcal{O}(0.01)$  and work on various two-point cross-correlations between photo- $z$  bins. Unless otherwise specified, we focus on the E-mode of galaxy ellipticities in cosmic shear surveys. The observed E-mode galaxy ellipticity is

$$\gamma_E^O = \gamma + I.$$

Here  $\gamma$  is the cosmic shear and  $I$  is the E-mode galaxy IA. The spatially uncorrelated (random) component of the galaxy shapes does not contribute in the nonzero lag correlation function, and the shape noise can be subtracted in the observed power spectrum. Therefore, for brevity we ignore this component. Together with the other observable, namely the galaxy surface number density, we can form three two-point auto/cross-correlations. The corresponding power spectra between the  $i$ th and the  $j$ th redshift bins are  $C_{ij}^{(1)}$  (the power spectrum between the observed(lensed) galaxy ellipticity),  $C_{ij}^{(2)}$  (the galaxy ellipticity-galaxy surface overdensity cross-power spectrum), and  $C_{ij}^{(3)}$  (the galaxy surface overdensity power

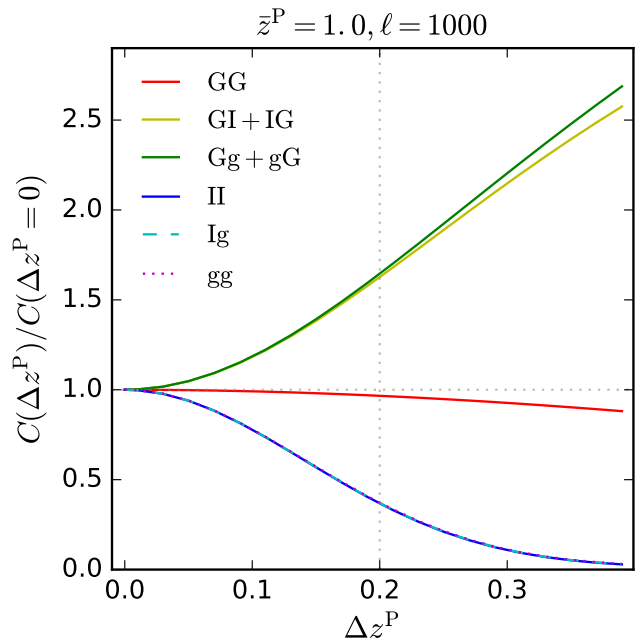


FIG. 1.— Classifications of various power spectra in the  $\Delta z^P$  space from the  $N$ -body simulation data. The cross-power spectra between galaxy IA/number overdensity and gravitational lensing increase with increasing  $\Delta z^P$ . In contrast, the power spectra between galaxy IA and number overdensity decreases with increasing  $\Delta z^P$ . The relative dependences are almost identical for II, Ig, and gg, and are therefore indistinguishable in the plot. The lensing power spectrum  $C^{GG}$  only weakly depends on  $\Delta z^P$ . This significant difference in the  $\Delta z^P$  dependence, along with the three scaling relations shown in Figures 2-4, are key ingredients of the proposed IA self-calibration technique.

spectrum). Notice that all three power spectra are symmetric with respect to the  $ij$  pair ( $C_{ij}^{(1,2,3)} = C_{ji}^{(1,2,3)}$ ).

$$\begin{aligned} C_{ij}^{(1)}(\ell) &= C_{ij}^{GG}(\ell) + C_{ij}^{II}(\ell) + C_{ij}^{GI}(\ell) + C_{ij}^{IG}(\ell), \\ C_{ij}^{(2)}(\ell) &= C_{ij}^{Gg}(\ell) + C_{ij}^{gG}(\ell) + 2C_{ij}^{Ig}(\ell), \\ C_{ij}^{(3)}(\ell) &= C_{ij}^{gg}(\ell). \end{aligned} \quad (1)$$

These measurable quantities are related to the underlying power spectra  $C_{ij}^{\alpha\beta}$ . Here,  $\alpha, \beta = G, I, g$  denote the gravitational shear, the IA, and the galaxy surface overdensity respectively.  $C_{ij}^{\alpha\beta}$  is the cross-power spectrum between the property  $\alpha$  of the  $i$ th redshift bin and the property  $\beta$  of the  $j$ th redshift bin. When  $\alpha = \beta$ ,  $C_{ji}^{\alpha\beta} = C_{ij}^{\alpha\beta}$ . However, when  $\alpha = G$  and  $\beta = I, g$ ,  $C_{ji}^{\alpha\beta} \neq C_{ij}^{\alpha\beta}$ .

In the measurement  $C_{ij}^{(1)}$ , the lensing power spectrum  $C_{ij}^{GG}$  is contaminated by both the II term and the GI term from the galaxy IA. Adding new measurements ( $C_{ij}^{(2,3)}$ ) on one hand provides extra constraints on IA, but on the other hand brings extra unknown quantities. Z10 found several scaling relations between these unknown quantities. They significantly reduce the degrees of freedom in Equation (1), and make  $C^{GG}$  solvable. These scaling relations are generic, arising from the very basic fact that both IA and the galaxy number density are intrinsic 3D fields, while cosmic shear is

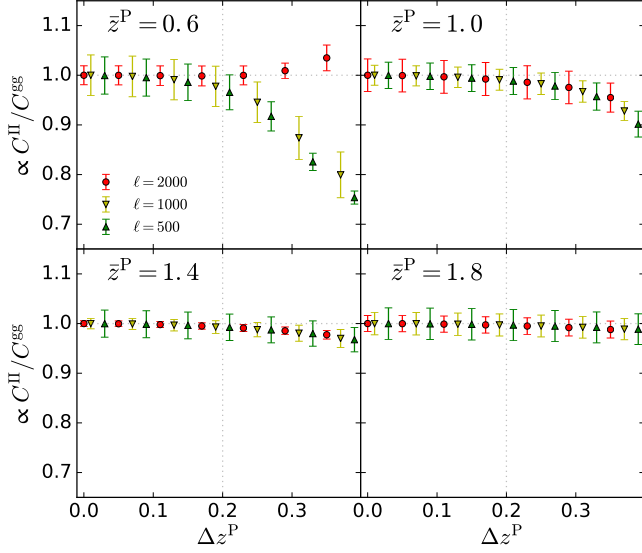


FIG. 2.— Verification of the scaling relation S1. S1 states that the ratio  $C^{\text{II}}(\Delta z^{\text{P}})/C^{\text{gg}}(\Delta z^{\text{P}})$  should be independent of  $\Delta z^{\text{P}}$ . Since the absolute amplitude is irrelevant, we scale the first data points (at  $\Delta z^{\text{P}} = 0$ ) to unity. S1 holds to an accuracy of  $\mathcal{O}(1)\%$  at  $\Delta z^{\text{P}} \leq 0.2$  and  $\bar{z}^{\text{P}} = 0.6$ . Its accuracy further improves toward higher  $\bar{z}^{\text{P}}$ .

the projection of a 3D field (matter density). The self-calibration based on them is therefore independent of IA modeling.

We denote the average redshift of galaxies in the  $i$ th redshift bin as  $z_i^{\text{P}}$ . Here the superscript ‘‘P’’ denotes the photometric redshift. The above power spectra then depend on both  $z_i^{\text{P}}$  and  $z_j^{\text{P}}$ . Such dependences can be re-expressed as the dependences on the mean redshift  $\bar{z}^{\text{P}} \equiv (z_i^{\text{P}} + z_j^{\text{P}})/2$ , and the redshift separation  $\Delta z^{\text{P}} \equiv z_j^{\text{P}} - z_i^{\text{P}}$ . With respect to these new arguments ( $\Delta z^{\text{P}}$ ,  $\bar{z}^{\text{P}}$  and  $\ell$ ), the scaling relations found in Z10 are

$$\begin{aligned} \text{S1} : C^{\text{II}}(\Delta z^{\text{P}}|\ell, \bar{z}^{\text{P}}) &\simeq A_{\text{II}}(\ell, \bar{z}^{\text{P}})C^{\text{gg}}(\Delta z^{\text{P}}|\ell, \bar{z}^{\text{P}}), \\ \text{S2} : C^{\text{Ig}}(\Delta z^{\text{P}}|\ell, \bar{z}^{\text{P}}) &\simeq A_{\text{Ig}}(\ell, \bar{z}^{\text{P}})C^{\text{gg}}(\Delta z^{\text{P}}|\ell, \bar{z}^{\text{P}}), \\ \text{S3} : C^{\text{GI}}(\Delta z^{\text{P}}|\ell, \bar{z}^{\text{P}}) + C^{\text{IG}}(\Delta z^{\text{P}}|\ell, \bar{z}^{\text{P}}) &\simeq A_{\text{GI}}(\ell, \bar{z}^{\text{P}}) \\ &\times [C^{\text{Gg}}(\Delta z^{\text{P}}|\ell, \bar{z}^{\text{P}}) + C^{\text{gG}}(\Delta z^{\text{P}}|\ell, \bar{z}^{\text{P}})]. \end{aligned} \quad (2)$$

The prefactors  $A_{\text{II}}$ ,  $A_{\text{Ig}}$ , and  $A_{\text{GI}}$  encode information of IA, but are hard to calculate from the first principle. What the scaling relations emphasize is that,  $A_{\text{II}}$ ,  $A_{\text{Ig}}$  and  $A_{\text{GI}}$  do not depend on  $\Delta z^{\text{P}}$ . In other words, the two sets of power spectra in the S1~S3 scaling relations have identical  $\Delta z^{\text{P}}$  dependence. Namely, the ratios (e.g.  $C^{\text{II}}/C^{\text{gg}}$  for fixed  $\ell$  and  $\bar{z}^{\text{P}}$ ) should be  $\Delta z^{\text{P}}$  independent. Z10 predicts that this should be valid at  $\Delta z^{\text{P}} \lesssim 0.2$ .

Fig. 1 shows the  $\Delta z^{\text{P}}$  dependences of the above power spectra measured from our simulation detailed later, for  $\ell = 1000$  and  $\bar{z}^{\text{P}} = 1.0$ . Although this figure indeed shows the validity of the above scaling relations, the major purpose is to demonstrate how the self-calibration works. The  $\Delta z^{\text{P}}$  dependences can be naturally classified into three categories, insensitive to details of IA.

- The lensing power spectrum only weakly depends on  $\Delta z^{\text{P}}$ , since the lensing kernel varies slowly with redshift. Based on this slow variation, Z10 also de-

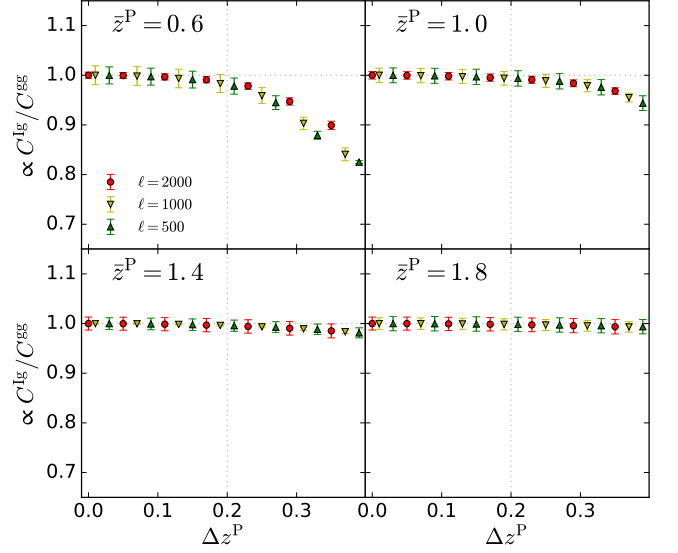


FIG. 3.— Verification of the scaling relation S2. It is similar to Figure 2, but for the ratios  $C^{\text{Ig}}/C^{\text{gg}}$ .

rived a generic scaling relation on the lensing power spectrum,

$$\frac{C^{\text{GG}}(\Delta z^{\text{P}}|\ell, \bar{z}^{\text{P}})}{C^{\text{GG}}(0|\ell, \bar{z}^{\text{P}})} \simeq 1 - A_{\text{GG}}(\ell, \bar{z}^{\text{P}})(\Delta z^{\text{P}})^2. \quad (3)$$

- $C^{\text{II}}$ ,  $|C^{\text{Ig}}|$ , and  $C^{\text{gg}}$  decrease quickly with increasing  $\Delta z^{\text{P}}$ . This is the natural consequence of short correlation length of the underlying 3D fields of IA and galaxy number density.
- In contrast, both  $|C^{\text{GI}} + C^{\text{IG}}|$  and  $C^{\text{Gg}} + C^{\text{gG}}$  increase quickly with increasing  $\Delta z^{\text{P}}$ . This is the natural consequence of higher lensing efficiency for larger source-lens separation.

Observationally, we can find redshift bin pairs of identical  $\bar{z}^{\text{P}}$  but different  $\Delta z^{\text{P}}$ . This allows us to separate the three categories of components using their different  $\Delta z^{\text{P}}$  dependences. Mathematically, with measurements of  $C^{(1,2,3)}$  at four or more  $\Delta z^{\text{P}}$ , we are able to solve for all unknowns in Equations (1)-(3). We then obtain  $C^{\text{GG}}$ , free of IA contamination, and independent of IA modeling. What’s more, we can get all the prefactors  $A_{\alpha\beta}$  in Equation (2)-(3) from all the observed quantities. So on the validation of these scaling relations we do not care the value of these prefactors  $A_{\alpha\beta}$  which indeed depend on the detailed IA physics.

Equation (3) has been verified unambiguously in Z10, since we already have a sufficiently accurate understanding of weak lensing statistics. The same paper also demonstrated the robustness of the S1~S3 scaling relations, but only for specific analytical/semianalytical IA models. The major remaining question is whether S1~S3 hold in more realistic situations. Therefore, we test these scaling relations with IA in numerical simulations.

### 3. THE $N$ -BODY SIMULATION AND DATA ANALYSIS

The  $N$ -body simulation we analyze has  $3072^3$  dark matter particles in a  $(600h^{-1}\text{Mpc})^3$  cosmic volume

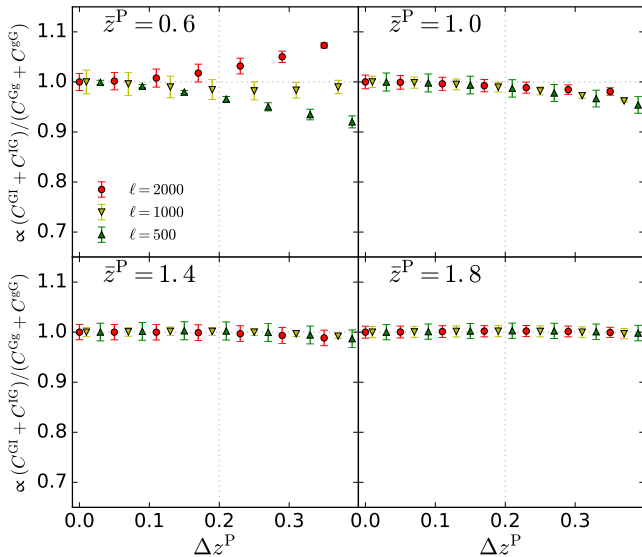


FIG. 4.— Verification of the scaling relation S3. It is similar to Figure 2, but for the ratios  $(C^{GI} + C^{IG})/(C^{Gg} + C^{gG})$ .

(hereafter J6610). It was run with a particle-particle-particle-mesh ( $P^3M$ ) code (Jing et al. 2007; Jing 2018). It adopts a flat  $\Lambda$ CDM cosmology with  $\Omega_m = 1 - \Omega_\Lambda = 0.268$ ,  $\Omega_b = 0.045$ ,  $h \equiv H_0/100/\text{kms}^{-1}\text{Mpc}^{-1} = 0.71$ ,  $\sigma_8 = 0.83$ , and  $n_s = 0.968$ . The dark matter halos are first identified using the friends-of-friends algorithm with a linking length 20% of the mean particle separation. All unbound particles are excluded in the final halo catalog. Our work only uses halos with at least 20 simulation particles. We restrict to the IA of early-type galaxies. Their IA is expected to arise from the ellipticities of host halos, up to a misalignment angle. The misalignment reduces the IA amplitude. However, it does not change the scaling relations S1~S3, as long as misalignments of galaxies in different halos are spatially uncorrelated. For this reason, we only need to test the scaling relations for halos and the results obtained automatically apply to early-type galaxies.

The halo ellipticities are defined (e.g. for projection onto the  $x$ - $y$  plane),

$$\epsilon_1 = \frac{I_{xx} - I_{yy}}{I_{xx} + I_{yy}}, \quad \epsilon_2 = \frac{2I_{xy}}{I_{xx} + I_{yy}}. \quad (4)$$

$I_{\alpha\beta}$  is the inertia tensor,

$$I_{\alpha\beta} = \frac{\sum_i^N w_i m_i (\alpha_i - \bar{\alpha})(\beta_i - \bar{\beta})}{\sum_i^N w_i m_i}. \quad (5)$$

Here  $\alpha_i$  and  $\beta_i$  are the coordinates of the  $i$ th halo particle in the simulation box, and  $\bar{\alpha}$  and  $\bar{\beta}$  are the coordinates of the halo center.  $m_i$  is the mass of the  $i$ th particle and  $w_i$  is its weighting. We adopt  $w_i = 1/r_i^2$ , where  $r_i$  is the distance of this particle to the halo center.  $I_{\alpha\beta}$  defined with such weighting is called the reduced inertia tensor. We then have the 3D distribution of ellipticities. With respect to the same line of sight, we can perform the E-B separation and obtain the 3D distribution of E-mode intrinsic ellipticity ( $I$ ).

There are two ways to calculate  $C^{\alpha\beta}(\ell)$  in the previous section. One way is to first make maps of  $\alpha = G, I, g$ , and

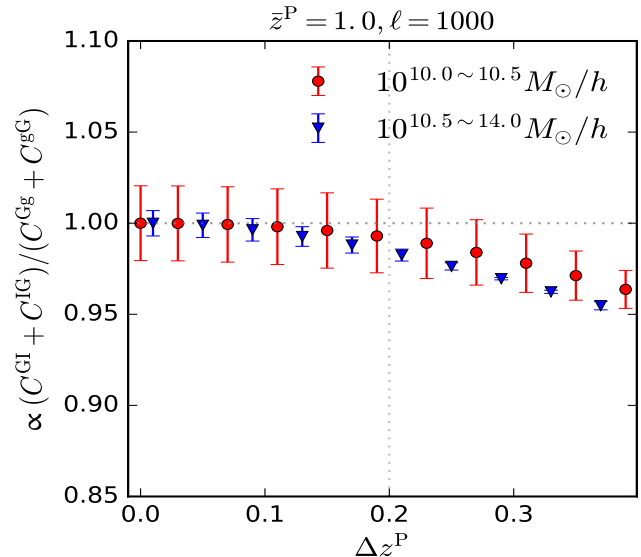


FIG. 5.— Scaling relations hold for different halo masses. This figure is similar to Figure 4, but for two halo mass bins.

then measure their cross-power spectra. This is straightforward. However, the large photo- $z$  error causes large scatter in the maps and we need to produce many of them to reduce the statistical fluctuation in  $C^{\alpha\beta}$ . Since these maps are not independent of each other, it is then difficult to quantify the statistical error in  $C^{\alpha\beta}$ . Another way is to first measure the corresponding 3D power spectra  $P^{\alpha\beta}(k, z)$  from the  $I$ ,  $\delta_m$ , and  $\delta_g$  fields and then apply the Limber integral to obtain  $C^{\alpha\beta}$ .

$$\frac{\ell^2}{2\pi} C^{\alpha\beta}(\Delta z^P | \ell, \bar{z}^P) = \frac{\pi}{\ell} \int_0^\infty \Delta_{\alpha\beta}^2 \left( k = \frac{\ell}{\chi(z)}, z \right) \times W_{\alpha\beta}(z, \Delta z^P, \bar{z}^P) \tilde{\chi}(z) \frac{H(z)}{H_0} dz. \quad (6)$$

Here,  $\Delta_{\alpha\beta}^2 \equiv k^3 P_{\alpha\beta}(k)/2\pi^2$  is the corresponding (dimensionless) 3D power spectrum variance.  $W_{\alpha\beta}$  is the corresponding weighting function, whose details are given in Z10.  $\tilde{\chi}(z) \equiv \chi/(c/H_0)$  is the comoving angular diameter distance in units of the Hubble radius.  $H(z)$  is the Hubble parameter at redshift  $z$ . Since the measurement of  $P^{\alpha\beta}$  uses all two-point information in the whole simulation box, the obtained  $C^{\alpha\beta}$  has minimal statistical fluctuations. Therefore, we will adopt this approach. For each line of sight  $(x, y, z)$ , we have an independent  $I$  field and its corresponding power spectra  $P^{I\alpha}$  and  $C^{I\alpha}$ . Comparing between the three lines of sight, we obtain the statistical errors of  $C^{I\alpha}$  and then quantify the accuracy of scaling relations. But we caution that such errorbars should not be used for cosmological constraints, since random shape noise is not included.

#### 4. VERIFICATIONS OF THE SCALING RELATIONS

We test the scaling relations (S1~S3) over a variety of redshifts and angular scales. For brevity, we only show the results at  $\ell = 500, 1000, 2000$  of interest in weak lensing cosmology. We also adopt  $\bar{z}^P = 0.6, 1.0, 1.4, 1.8$ , which cover a large range of accessible source redshifts

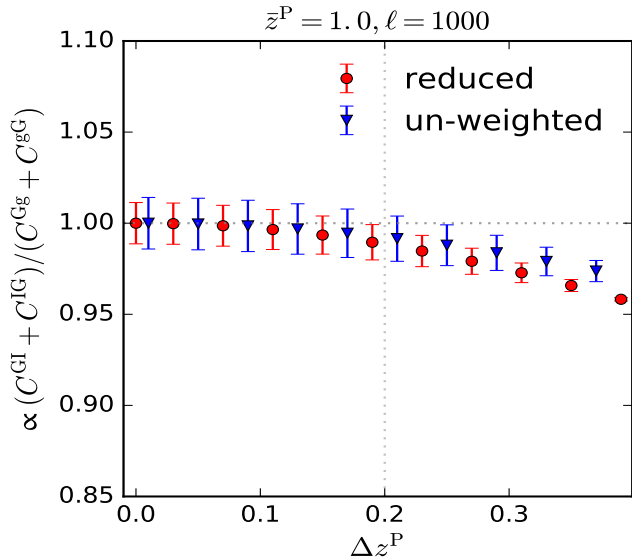


FIG. 6.— Scaling relations hold for different definitions of halo ellipticities. This figure is similar to Figure 4, but for comparing two different ways of calculating the inertia tensor (reduced and unweighted) and the halo ellipticities.

for most weak lensing surveys.

Fig. 2 plots the ratio  $C^{\text{II}}(\Delta z^{\text{P}})/C^{\text{GG}}(\Delta z^{\text{P}})$  as a function of  $\Delta z^{\text{P}}$  for fixed  $\ell$  and  $\bar{z}^{\text{P}}$  with values listed above. If the scaling relation S1 holds, the ratios should be horizontal lines (independent of  $\Delta z^{\text{P}}$ ). Fig. 2 shows that this is indeed the case. The overall accuracy reaches  $\mathcal{O}(1)\%$  at  $\Delta z^{\text{P}} \lesssim 0.2$ . The accuracy is better for larger  $\ell$  and higher  $\bar{z}^{\text{P}}$ , as predicted in Z10. For example, 1% accuracy remains for  $\Delta z^{\text{P}} \leq 0.3$ , for  $\ell = 2000$  and  $0.6 \leq \bar{z}^{\text{P}} \leq 1.8$ , and for  $500 \leq \ell \leq 2000$  and  $\bar{z}^{\text{P}} = 1.4/1.8$ .

Fig. 3 shows the ratios  $C^{\text{IG}}/C^{\text{GG}}$ , and verifies the scaling relation S2. Fig. 4 shows the ratios  $(C^{\text{GI}} + C^{\text{IG}})/(C^{\text{GG}} + C^{\text{GG}})$  and verifies the scaling relation S3. The accuracies of S2 and S3 also reach  $\mathcal{O}(1)\%$ , comparable to that of S1. Therefore, we verify the scaling relations for halo ellipticities. The ellipticities of early-type galaxies can be well described by the halo ellipticities and a spatially uncorrelated misalignment angle between halos and galaxies (Okumura & Jing 2009; Okumura et al. 2009). Such misalignment does not affect the S1~S3 scaling relations. We then conclude that the predicted scaling relation S1~S3 are accurate to the  $\mathcal{O}(1)\%$  level when  $\Delta z^{\text{P}} \lesssim 0.2$ , for both halo and galaxy ellipticities. Such a level of accuracy is sufficient for accurate removal of IA in cosmic shear power spectrum measurement.

#### 4.1. The universality of the scaling relations

The scaling relations S1~S3 are universal in several ways. They hold for halos of different mass. We split halos into two mass bins,  $10^{10} < M/(M_{\odot}/h) < 10^{10.5}$  and  $10^{10.5} < M/(M_{\odot}/h) < 10^{14}$  and redo the tests.<sup>8</sup>

<sup>8</sup> Jing (2002) pointed out for halos with too few particles, the ellipticity correlation will be underestimated, and the underestimation amounts to a factor of two for halos of 20 simulation particles. This underestimation can be described by an extra misalignment. Therefore, it does not change the scaling relations. The low-mass halo sample verifies this argument.

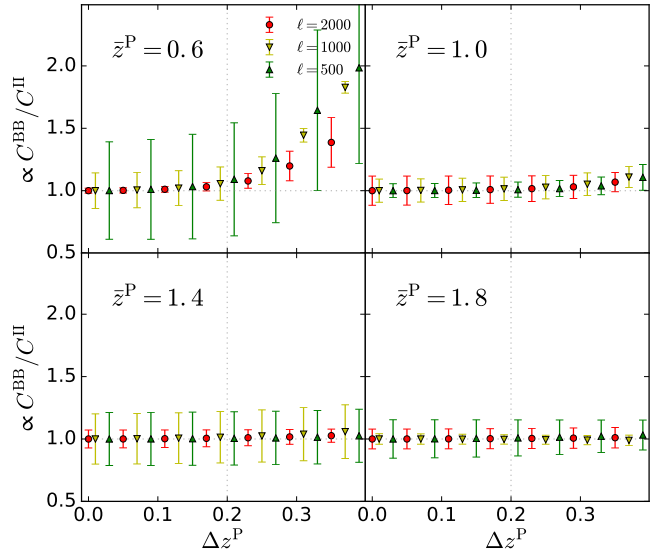


FIG. 7.— Verification of the B-mode scaling relation proposed in Eq. 7. It is similar to Fig. 2, but for the B-E relation. These new scaling relations are useful when studying the IA B-mode as a tracer of the large-scale structure and when calibrating IA in the weak lensing measurement. Notice that errorbars at different  $\Delta z^{\text{P}}$  are correlated due to the common 3D power spectra shared in the Limber integral (Equation (6)).

For brevity, we only show the test against S3 at  $\bar{z}^{\text{P}} = 1.0$  and  $\ell = 1000$  (Fig. 5). In addition, scaling relations S1, S2, and other  $\bar{z}^{\text{P}}$ ,  $\ell$  have similar conclusions. Both halo samples obey the scaling relation S3 to  $\mathcal{O}(1)\%$  accuracy at  $\Delta z^{\text{P}} \leq 0.2$  ( $\mathcal{O}(5)\%$  accuracy at  $\Delta z^{\text{P}} \leq 0.4$ ).

They hold for different weighting  $w_i$  in the definition of the inertial tensor and the ellipticities (Eq. 5). Previous works (e.g. Pereira et al. 2008; Joachimi et al. 2013; Hilbert et al. 2017) showed that ellipticities can differ significantly in the inner and outer regions of halos/galaxies and therefore depend significantly on the weighting  $w_i$ . However, this does not affect the scaling relations S1~S3. Figure 6 shows the tests of S3 adopting  $w_i = 1$  and compare it with the case of  $w_i = 1/r_i^2$  adopted previously. Despite the strong dependence of IA on the weighting, the scaling relations still hold. This further supports the argument in Z10 that scaling relations S1~S3 are generic and do not rely on the details of IA.

They are also insensitive to details of photo- $z$  error distribution. All the power spectra  $C^{\alpha\beta}$  are affected by the photo- $z$  errors. But since the photo- $z$  errors affect both the left- and right-hand sides in basically the same way, the scaling relations S1~S3 are insensitive to the photo- $z$  errors. The above tests adopt a double Gaussians PDF for photo- $z$  errors, detailed in Z10. We have checked that, for a single Gaussian or non-Gaussian PDF, the scaling relations also hold.

#### 4.2. Scaling relations of B-mode IA

Unlike cosmic shear, which has negligible B-mode, B-mode of IA is usually non-negligible (e.g. Crittenden et al. (2001, 2002); Hirata & Seljak (2004); Heymans et al. (2006)). By its symmetry property, B-mode is only correlated with itself and the only nonvanishing two-point statistics is its auto power spectrum  $C^{\text{BB}}$ . Based on the same argument in Z10, we expect the following three



scaling relations,

$$\begin{aligned} S4 : C^{\text{BB}}(\Delta z^{\text{P}}|\ell, \bar{z}^{\text{P}}) &\simeq A_{\text{BE}}(\ell, \bar{z}^{\text{P}})C^{\text{II}}(\Delta z^{\text{P}}|\ell, \bar{z}^{\text{P}}) \\ &\simeq A_{\text{BIg}}(\ell, \bar{z}^{\text{P}})C^{\text{Ig}}(\Delta z^{\text{P}}|\ell, \bar{z}^{\text{P}}) \\ &\simeq A_{\text{Bg}}(\ell, \bar{z}^{\text{P}})C^{\text{gg}}(\Delta z^{\text{P}}|\ell, \bar{z}^{\text{P}}). \end{aligned} \quad (7)$$

The same simulation also verifies the above three new scaling relations, and for brevity we only use one of the tests (Fig. 7). These scaling relations are useful in both separating shape measurement errors in B-mode (e.g. RCSLenS (Hildebrandt et al. 2016), KiDS-450 (Hildebrandt et al. 2017)) and calibrating the IA E-mode .

## 5. DISCUSSION AND SUMMARY

We carry out comprehensive tests of the three scaling relations useful for the IA self-calibration proposed in Z10. We conclude that these scaling relations are valid for all investigated angular scales  $\ell$ , mean-source redshifts  $\bar{z}^{\text{P}}$ , source redshift separations  $\Delta z^{\text{P}}$ , halo masses, weightings in the halo ellipticity definition, and photo- $z$  error distribution. The tests are for halo ellipticities. But since misalignment between ellipticities of early-type galaxies and host halos does not alter these scaling relations, the same conclusion applies to galaxy ellipticities. This makes the proposed IA self-calibration complete on the theory side, and makes it ready for application to real data analysis of galaxy ellipticities and cosmic shear.

In the original proposal of Z10, only scaling relations related to E-mode ellipticity are discussed. The same argument naturally leads to scaling relations of B-mode ellipticity. We list these scaling relations and verify them

in §4.2.

There are further complexities to take care. For example, there are different estimators of measuring the ellipticity correlations. We adopt the pixel-based estimator. We also need to check the standard estimator (e.g. Munshi et al. 2008; Schmidt et al. 2009; Heymans et al. 2012). Nevertheless, since the derivation of the scaling relations is not restricted to a specific estimator, we expect that these scaling relations should hold as well. Furthermore, the tests done for halos in  $N$ -body simulations should be extended to galaxies in hydrodynamical simulations. This will allow us to more robustly check the dependence on galaxy types.

## ACKNOWLEDGEMENTS

We thank Zheng Zheng, Jun Zhang, Huanyuan Shan, Le Zhang, Ji Yao, Xi Kang, and Peng Wang for useful discussions. This work was supported by the National Key Basic Research and Development Program of China (No. 2018YFA0404504), the National Science Foundation of China (11773048, 11403071, 11621303, 11433001, 11653003, 11533006, 11222325, 11033006 and 11320101002), the National Basic Research Program of China (2015CB857001, 2015CB857003), the Knowledge Innovation Program of CAS (KJXC2-EW-J01), Shanghai talent development funding (No. 2011069) and Shanghai Key Laboratory Grant (No.11DZ2260700). This work made use of the High Performance Computing Resource in the Core Facility for Advanced Research Computing at Shanghai Astronomical Observatory.

## REFERENCES

- Abbott, T., Abdalla, F. B., Allam, S., et al. 2016, *Phys. Rev. D*, 94, 022001
- Blazek, J., McQuinn, M., & Seljak, U. 2011, *JCAP*, 5, 010
- Blazek, J., Vlah, Z., & Seljak, U. 2015, *JCAP*, 8, 015
- Blazek, J., MacCrann, N., Troxel, M. A., & Fang, X. 2017, arXiv:1708.09247
- Bridle, S., & King, L. 2007, *New Journal of Physics*, 9, 444
- Brown, M. L., Taylor, A. N., Hambly, N. C., & Dye, S. 2002, *MNRAS*, 333, 501
- Catelan, P., Kamionkowski, M., & Blandford, R. D. 2001, *MNRAS*, 320, L7
- Crittenden, R. G., Natarajan, P., Pen, U.-L., & Theuns, T. 2001, *ApJ*, 559, 552
- Crittenden, R. G., Natarajan, P., Pen, U.-L., & Theuns, T. 2002, *ApJ*, 568, 20
- Croft, R. A. C., & Metzler, C. A. 2000, *ApJ*, 545, 561
- Heavens, A., Refregier, A., & Heymans, C. 2000, *MNRAS*, 319, 649
- Heymans, C., & Heavens, A. 2003, *MNRAS*, 339, 711
- Heymans, C., White, M., Heavens, A., Vale, C., & van Waerbeke, L. 2006, *MNRAS*, 371, 750
- Heymans, C., Van Waerbeke, L., Miller, L., et al. 2012, *MNRAS*, 427, 146
- Heymans, C., Grootjans, E., Heavens, A., et al. 2013, *MNRAS*, 432, 2433
- Hilbert, S., Xu, D., Schneider, P., et al. 2017, *MNRAS*, 468, 790
- Hildebrandt, H., Choi, A., Heymans, C., et al. 2016, *MNRAS*, 463, 635
- Hildebrandt, H., Viola, M., Heymans, C., et al. 2017, *MNRAS*, 465, 1454
- Hirata, C. M., Mandelbaum, R., Seljak, U., et al. 2004, *MNRAS*, 353, 529
- Hirata, C. M., & Seljak, U. 2004, *Phys. Rev. D*, 70, 063526
- Hirata, C. M., Mandelbaum, R., Ishak, M., et al. 2007, *MNRAS*, 381, 1197
- Hui, L., & Zhang, J. 2008, *ApJ*, 688, 742-756
- Jing, Y. P. 2002, *MNRAS*, 335, L89
- Jing, Y. P., Suto, Y., & Mo, H. J. 2007, *ApJ*, 657, 664
- Jing, Y. P., 2018, arxiv: 1807.06802
- Joachimi, B., & Schneider, P. 2008, *A&A*, 488, 829
- Joachimi, B., & Schneider, P. 2009, *A&A*, 507, 105
- Joachimi, B., Mandelbaum, R., Abdalla, F. B., & Bridle, S. L. 2011, *A&A*, 527, A26
- Joachimi, B., Semboloni, E., Hilbert, S., et al. 2013, *MNRAS*, 436, 819
- Joudaki, S., Blake, C., Heymans, C., et al. 2017, *MNRAS*, 465, 2033
- King, L., & Schneider, P. 2002, *A&A*, 396, 411
- King, L. J., & Schneider, P. 2003, *A&A*, 398, 23
- King, L. J. 2005, *A&A*, 441, 47
- Kirk, D., Bridle, S., & Schneider, M. 2010, *MNRAS*, 408, 1502
- Lee, J., & Pen, U.-L. 2001, *ApJ*, 555, 106
- Mandelbaum, R., Hirata, C. M., Ishak, M., Seljak, U., & Brinkmann, J. 2006, *MNRAS*, 367, 611
- Mandelbaum, R., Blake, C., Bridle, S., et al. 2011, *MNRAS*, 410, 844
- Munshi, D., Valageas, P., van Waerbeke, L., & Heavens, A. 2008, *Phys. Rep.*, 462, 67
- Okumura, T., & Jing, Y. P. 2009, *ApJ*, 694, L83
- Okumura, T., Jing, Y. P., & Li, C. 2009, *ApJ*, 694, 214
- Pereira, M. J., Bryan, G. L., & Gill, S. P. D. 2008, *ApJ*, 672, 825-833
- Schmidt, F., Rozo, E., Dodelson, S., Hui, L., & Sheldon, E. 2009, *ApJ*, 702, 593
- Schneider, M. D., & Bridle, S. 2010, *MNRAS*, 402, 2127
- Singh, S., Mandelbaum, R., & More, S. 2015, *MNRAS*, 450, 2195
- Singh, S., & Mandelbaum, R. 2016, *MNRAS*, 457, 2301
- Takada, M., & White, M. 2004, *ApJ*, 601, L1
- Troxel, M. A., & Ishak, M. 2012a, *MNRAS*, 419, 1804
- Troxel, M. A., & Ishak, M. 2012b, *MNRAS*, 423, 1663
- Troxel, M. A., & Ishak, M. 2012c, *MNRAS*, 427, 442
- Troxel, M. A., & Ishak, M. 2015, *Phys. Rep.*, 558, 1
- Troxel, M. A., MacCrann, N., Zuntz, J., et al. 2017, arXiv:1708.01538
- Tugendhat, T. M., & Schäfer, B. M. 2018, *MNRAS*, 476, 3460
- van Uitert, E., & Joachimi, B. 2017, *MNRAS*, 468, 4502
- Wei, C., Li, G., Kang, X., et al. 2018, *ApJ*, 853, 25
- Xia, Q., Kang, X., Wang, P., et al. 2017, *ApJ*, 848, 22
- Yao, J., Ishak, M., Lin, W., & Troxel, M. 2017, *JCAP*, 10, 056
- Zhang, P. 2010a, *ApJ*, 720, 1090
- Zhang, P. 2010b, *MNRAS*, 406, L95